

# Numerical simulation of growth of *Escherichia coli* in unsaturated porous media

P. Hron<sup>1</sup>, D. Jost<sup>2</sup>, P. Bastian<sup>1</sup>, C. Gallert<sup>3</sup>, J. Winter<sup>2</sup>, O. Ippisch<sup>1,4</sup>

<sup>1</sup>University of Heidelberg, Interdisciplinary Center for Scientific Computing, Im Neuenheimer Feld 368, 69120 Heidelberg, Germany

<sup>2</sup>Karlsruhe Institute of Technology, Institut für Ingenieurbiologie und Biotechnologie des Abwassers, Am Fasanengarten Geb. 50.31, 76131 Karlsruhe, Germany

<sup>3</sup>University of Applied Science Hochschule Emden/Leer, Faculty of Technology, Microbiology – Biotechnology, Constantiaplatz 4, 26723 Emden, Germany

<sup>4</sup>Clausthal University of Technology, Department of Mathematics, Erzstraße 1, 38678 Clausthal-Zellerfeld, Germany

Email: pavel.hron@iwr.uni-heidelberg.de

## Abstract

A model for the aerobic and anaerobic growth of *Escherichia coli* (HB101 K12 pGLO) depending on the concentration of oxygen and DOC as substrate has been developed based on laboratory batch experiments. Using inverse modelling to obtain optimal sets of parameters, it could be shown that a model based on a modified double Contois kinetic can predict cell densities, organic carbon utilisation, oxygen transfer and utilisation rates for a large number of experiments under aerobic and anaerobic conditions with a single unique set of parameters.

The model was extended to describe growth of *E. coli* in unsaturated porous media, combining diffusion, phase exchange and microbiological growth. Experiments in a Hele-Shaw cell, filled with quartz sand, were conducted to study bacterial growth in the capillary fringe above a saturated porous medium. Cell density profiles in the Hele-Shaw cell were predicted with the growth model and the parameters from the batch experiments without any further calibration. They showed a very good qualitative and quantitative agreement with cell densities determined from samples taken from the Hele-Shaw cell by re-suspension and subsequent counting. Thus it could be shown, that it is possible to successfully transfer growth parameters from batch experiments to porous media for both aerobic and anaerobic conditions.

## 1. Introduction

Bacterial growth and activity in the vadose zone is a topic of growing interest for ecologists and soil scientists within the last decade [1, 2, 3, 4]. The knowledge about microbial processes under unsaturated conditions was used e.g. for in situ bioremediation methods [5, 6] or for sand filter techniques [7]. However, there is still the need for research on bacterial growth, i.e. in a complex region as the capillary fringe [8]. We define the capillary fringe (CF) broader than the classical definition only including the zone where the gas phase is discontinuous down to the zero capillary pressure isosurface, but as the region which is dominated by capillary rise from the groundwater table.

Bacterial growth in soil usually depends on bioavailable water content [9, 10], temperature [11, 12] and other physical or environmental parameters like pressure, pH [13] or biogeochemical redox processes [14]. In addition to water saturation, the most important factors controlling bacterial growth are the availability of substrate or nutrients [15] and the availability of electron acceptors like oxygen for aerobic or facultative anaerobic bacteria [16] and nitrate for anaerobic respiration [17].

Normally most of the nutrients are transported in the soil via percolating water after rainfall. The nutrient supply in the soil then is highest at preferential flow paths of the water. Thus bacteria induce "hot spots of growth" at these locations [18]. Besides these preferential flow paths the CF offers attractive growth

conditions for aerobic soil microorganisms [19, 20, 21]. Water is sufficiently available due to capillary rise and oxygen is delivered by diffusion in the vadose zone. Nutrients or Nitrate as alternative electron acceptor are replenished by percolating water.

The major aim of this paper is the description of bacterial growth in the CF as a potential hot spot for the degradation of subsurface contaminants either by aerobic processes in the unsaturated part of the CF or by anaerobic processes in the fully saturated zone.

In some previous laboratory experiments *Pseudomonas putida*, a typical soil bacterium, was used to study biodegradation of toluene within a contaminant-plume [22, 23] in a saturated porous medium with a flow through chamber. In this study *Escherichia coli*, an indicator bacterium for faecal pollution of the environment [24], was used. *E. coli* can grow under anaerobic and aerobic conditions [25, 26] which both have to be considered in an appropriate growth model. Such a growth model will be developed and parametrised based on batch experiments, and applied to predict experiments in a flow through cell with conditions representing the capillary fringe. The simulations are performed without any additional calibration of the estimated parameters.

## 2. Batch experiments

### 2.1. Principal experimental setup

To understand the growth of *E. coli* and to describe the population dynamics (such as cell densities and their dependence on substrate concentrations), a number of different batch-culture experiments under varying conditions were performed. *E. coli* normally has its growth optimum at a rather high temperature ( $\approx 37^\circ\text{C}$ ) [27, 28], whereas for our experiments, the cells were cultivated at room temperature  $21 \pm 1^\circ\text{C}$  which is closer to natural conditions.

### 2.2. Bacterial strain and its cultivation

For all experiments in this study the Gram-negative, motile bacterial strain *E. coli* HB101 K12 pGLO (Bio-Rad, Germany) was used. The strain was cultivated in autoclaved LB medium (with Tryptose 10, Yeast extract 5 and NaCl  $10\text{ g l}^{-1}$ ) at a starting pH of 7.0-7.2, and a dissolved organic carbon (DOC) concentration of  $6.8\text{ g l}^{-1}$ . The active cells of this strain generate a green fluorescent protein (GFP) after addition of  $3\text{ mmol l}^{-1}$  Arabinose (sterile filtered, Roth, Germany). Previous experiments showed that the *E. coli* strain could not use L(+)-Arabinose for energy generation or biomass production. Due to a linkage with the *ampR-gen*, the strain is also resistant against Ampicillin ( $0.3\text{ mmol l}^{-1}$

of which was added). While the fluorescence was not used in the work described in this paper, the Arabinose was still added as it will be used in future work.

### 2.3. Aerobic growth of *E. coli*

For the aerobic experiments cotton plugged shake flasks filled with 30 ml of the different solutions described below were used and approximately  $2.3 \cdot 10^7\text{ cells ml}^{-1}$  (taken from a freshly grown culture) were added. Duplicate culture assays were shaken with a frequency of 200 rpm. The optical density (OD) at 578 nm was measured after inoculation and after every 1 h during the initial phase (log-phase) of bacterial growth and at several points in time afterwards with a photometer (M501 Single Beam Scanning Spectrophotometer, Camspec, UK) to get the growth curves. Calibration experiments showed that OD values were linear dependent on the cell density.

The LB medium was used pure and diluted with 0.9% NaCl solution to  $1/2$  (1:1),  $1/5$  (1:4) and  $1/10$  (1:9) of the original concentration. The oxygen concentration in the air phase was kept constant at 20%.

In addition the biomass (dry weight) of *E. coli* cells after the growth phase was measured gravimetrically for each replicate. Cell suspensions were centrifuged (8 min, 12 k rpm) and washed once with autoclaved, deionised water after discarding the supernatant medium. After a second centrifugation, the cells were resuspended in deionised water, filled in ceramic crucibles and the dry weight (dw) of the biomass from each flask was determined.

The DOC concentration of both, the original medium and the discarded medium from the centrifuge, were measured with a "High TOC" carbon analyser (Elementar, Hanau, Germany) and the amount of DOC consumed was determined.

Cell suspensions in undiluted LB medium reached their maximal OD of approx. 4.4 after 24 h of growth (Fig. 1). *E. coli* cells in suspensions with a lower DOC concentration reached their highest OD later (after up to 32 h). The *E. coli* cells consumed only about 30% of the available DOC, which means a maximal DOC consumption of  $2.0\text{ g l}^{-1}$  for the cells grown in undiluted LB medium.

The initial biomass (as average value of the dry weight of the *E. coli* cells in two samples) was  $0.02\text{ g dw l}^{-1}$ , the increase after 24 h was  $1.69\text{ g dw l}^{-1}$  for growth in undiluted LB medium,  $0.9\text{ g dw l}^{-1}$  in 1:1 diluted LB medium,  $0.42\text{ g dw l}^{-1}$  in 1:4 and  $0.27\text{ g dw l}^{-1}$  in a 1:9 dilution.

#### 2.4. Anaerobic growth of *E. coli*

For the anaerobic experiments closed serum bottles with a total volume of 120 ml, each filled with 20 ml of one of the four different solutions and a nitrogen atmosphere (HiQ Nitrogen 5.0 Linde Gas, Germany) were autoclaved. After an inoculation with  $2.0 \cdot 10^7$  cells  $\text{ml}^{-1}$  the experiments were conducted under the same conditions as for aerobic growth (only without continuous shaking).

The amount of consumed or metabolised DOC was estimated on the basis of the hydrogen (according to [29]) and fatty acid production. The metabolites of the mixed acid fermentation were measured after 48 h with a gas chromatograph (Varian 431-GC) and a mass spectrometer (Varian 210-MS, Agilent Technologies, USA). The OD was again measured at the start of the experiment, after every hour in the log-phase and at some specific points afterwards, and the biomass increase was measured for all samples at the end of the experiment.

As expected, the growth of *E. coli* under anaerobic conditions was slower than under aerobic conditions as a consequence of the lower efficiency of substrate fermentation. A maximal OD of 0.45 was reached after approximately 24 h in undiluted LB medium. About 30% of the available DOC was consumed or converted to metabolites. After 24 h the biomass increase was  $0.28 \text{ g dw l}^{-1}$  for the cells grown in undiluted LB medium.

#### 2.5. Aerobic growth of *E. coli* under different oxygen concentrations

To determine the dependence of the growth rate on oxygen availability, experiments with different oxygen concentrations were conducted in closed 50 ml glass vessels filled with 20 ml of undiluted LB medium only. Before and after the addition of  $2.3 \cdot 10^7$  cells  $\text{ml}^{-1}$ , each vessel was flushed (with a flow rate of approximately  $1.5 \text{ l h}^{-1}$ ) with a mixture of different ratios of sterile artificial air<sup>1</sup> and pure nitrogen<sup>2</sup> to achieve oxygen concentrations of 0, 1, 2, 3.5, 4, 6, 10, 15 and 20%. To achieve these concentrations, dosing valves for low flow (Swagelok, Germany) were used for each vessel. To guarantee optimal air input, the medium was stirred with approx 200 rpm on a magnetic stirring plate (Variomag, USA). 50  $\mu\text{L}$  of 100 times diluted silicon-antifoam emulsion (Carl Roth GmbH, Karlsruhe, Germany) was added. Oxygen concentrations at regular time intervals were measured by a non-invasive optode technique [30].

The experiments showed that the growth rate of *E. coli* under aerobic conditions was highly dependent on sufficient availability of oxygen. At concentrations

of 20-21%  $\text{O}_2$  (corresponding to ordinary air) and 6%, the OD values were almost identical. Below an oxygen concentration of 3.5%, the growth rate decreased significantly. Despite the continuous shaking the optode measurements showed a lower oxygen content in the liquid phase than in equilibrium with the gas phase. The consumption of oxygen in water thus was faster than oxygen dissolution from air.

#### 2.6. Oxygen consumption

To measure oxygen consumption and biomass production, experiments were conducted in closed serum bottles filled with 10 ml of liquid and 110 ml sterile artificial air to guarantee an initial oxygen concentration of 20% or a total oxygen volume of approx. 22 ml, respectively.

Undiluted LB medium and two dilutions (1:4 and 1:9) were used, to assess the influence of nutrient availability on oxygen consumption. The bacterial inoculum was the same as in the previously described experiments and the bottles were again shaken with 200 rpm. The oxygen concentration in the liquid phase was again measured with a non-invasive optode technique. After 24 hours a sample was taken from the head space of each bottle and the oxygen concentration in the gas phase was measured with a gas chromatograph (Chrompack, model CP 9001, Engstingen, Germany) and total biomass production was determined gravimetrically.

After 52 h the biomass of *E. coli* cells grown in 1:4 diluted LB was  $0.36 \text{ g l}^{-1}$  and  $0.23 \text{ g l}^{-1}$  in 1:9 diluted LB medium. The oxygen consumption for *E. coli* in 20 ml 1:4 diluted LB was  $19.7 \text{ mg O}_2$  and for cells grown in 1:9 diluted LB a value of  $10.1 \text{ mg O}_2$  was measured.

#### 2.7. Conclusions from the batch experiments

The following conclusions on the main factors controlling growth of *E. coli* have been obtained from the batch experiments:

- Cell growth is faster in presence of oxygen. This is a consequence of the higher energy efficiency of aerobic respiration compared to anaerobic fermentation.
- Anaerobic growth takes place only if the amount of available oxygen is very low. If enough oxygen is available only aerobic respiration is active.
- Oxygen is still consumed after the growth phase (log-phase), when all convertible DOC is already depleted. The necessary nutrients are most probably taken from intracellular resources.

<sup>1</sup>20% oxygen and 80% nitrogen

<sup>2</sup>HiQ Nitrogen 5.0 from Linde Gas, Germany

- At high cell and DOC concentrations the dissolution of oxygen in water is slower than oxygen consumption.
- In all batch experiments only up to 30 % of the total DOC was consumed or converted for both the aerobic and the anaerobic growth.

### 3. Modelling microbial growth

Based on the results of the batch-culture experiments models for the prediction of the growth of *E. coli* were derived depending on oxygen and DOC availability based on common approaches in the literature and their performance was compared for reproduction of all experimental data with a single set of parameters.

#### 3.1. Substrate-limited kinetics

Various mathematical models have been proposed to quantitatively describe microbial growth kinetics, see [31, 32, 33, 34, 35, 36].

The biomass concentration under anaerobic conditions is described by a first order differential equation relating the change of the biomass concentration over time to the current biomass concentration  $c_{l,X}$  multiplied with a specific growth rate  $\mu_{an}^*$

$$\frac{dc_{l,X}}{dt} = \mu_{an}^* c_{l,X}.$$

$\mu_{an}^*$  is the product of a maximal specific growth rate  $\mu_{max,an}$  and a relative specific growth rate.  $\mu_{max,an}$  is a characteristic of all organisms and it is related to their ability to reproduce. It is simply defined as the increase of biomass per unit of time under optimal conditions (no limiting nutrients).

Common growth kinetics expressing the relative speed of growth depending on the concentration  $s_i$  of a single substrate are given by:

$$\text{Monod} \quad \frac{s_i}{K_{s_i} + s_i}, \quad (1)$$

$$\text{Moser} \quad (1 + K_{s_i} s_i^{-\lambda_i})^{-1}, \quad (2)$$

$$\text{Tessier} \quad 1 - \exp\left(-\frac{s_i}{K_{s_i}}\right), \quad (3)$$

$$\text{Contois} \quad \frac{s_i}{B_i c_{l,X} + s_i}. \quad (4)$$

The substrate affinity constant (half-saturation constant)  $K_{s_i}$  can be interpreted as a reflection of the affinity of the bacterial cell towards the substrate  $s_i$ . It represents the substrate concentration at which growth with half the maximal speed occurs. Moser's constant  $\lambda_i$  and the constant  $B_i$  in the Contois model do not have direct biological meaning. In our case  $s_i = c_{l,S}$ ,

which denotes the concentration of bioconvertible nutrients and is only a part of the total DOC in the medium.

Together with a Monod kinetic (1) we obtain for example

$$\mu_{an}^* = \mu_{max,an} \frac{c_{l,S}}{K_{S,an} + c_{l,S}}. \quad (5)$$

#### 3.2. Multiple-substrate kinetics

While under anaerobic conditions the growth of *E. coli* or other facultative anaerobic microorganisms depend only on the bioavailable organic carbon concentration, under aerobic conditions the oxygen concentration  $c_{l,O_2}$  in the liquid phase has to be taken into account as well. [37] used a double Monod model to describe this double nutrient limitation for the growth of *Pseudomonas denitrificans*. It combines two Monod kinetics in a multiplicative form. The (aerobic) specific growth rate with a double Monod model is given by

$$\mu_a = \mu_{max,a} \frac{c_{l,S}}{K_{S,a} + c_{l,S}} \frac{c_{l,O_2}}{K_{O_2} + c_{l,O_2}}. \quad (6)$$

In both growth models (5) and (6), the Monod kinetics can be substituted with each of the other models of the relative specific growth rate (2)-(4).

#### 3.3. Combination of aerobic and anaerobic growth

While aerobic growth of *E. coli* cells is already occurring at low oxygen concentrations, anaerobic growth might still be important. As aerobic respiration is much more efficient, we assume that only aerobic growth occurs if  $\mu_a$  is higher than the growth rate for purely anaerobic growth under the same substrate limitation ( $\mu_a \geq \mu_{an}^*$ ). Under these assumptions the specific growth rate function for anaerobic growth in presence of oxygen  $\mu_{an}$  can be defined as

$$\mu_{an} = \max(\mu_{an}^* - \mu_a, 0), \quad (7)$$

The total growth rate  $\mu = \mu_a + \mu_{an}$  is then a non-decreasing function of  $c_{l,O_2}$  for constant  $c_{l,S}$ , where only the ratio between aerobic and anaerobic growth is changing.

#### 3.4. Mass balance equations

We consider a constant volume  $V_l$  of liquid phase (culture medium) and gas phase  $V_g$ . As there is no injection or removal of cells during the experiment, the balance equation for the cell density  $c_{l,X}$  is given by

$$\frac{dc_{l,X}}{dt} = (\mu_a + \mu_{an} - r_d) c_{l,X}, \quad (8a)$$

where  $r_d$  is the decay rate. The generic balance equation for the consumable substrate  $c_{l,S}$  has the form

$$\frac{dc_{l,S}}{dt} = - \left( \frac{\mu_a}{Y_{S,a}} + \frac{\mu_{an}}{Y_{S,an}} \right) c_{l,S}, \quad (8b)$$

where the yield coefficients  $Y_{S,a}$  and  $Y_{S,an}$  are the link between growth rate and substrate utilisation, a measure for the efficiency of the conversion of a substrate into biomass.

Oxygen transfer between liquid and gas phase occurs at the interface between both phases. For gases with a low solubility, like oxygen in water, the local equilibrium concentration of oxygen in water  $c_{l,O_2}^*$  can be described by Henry's law

$$c_{l,O_2}^* = k_H p_{O_2},$$

where  $k_H$  is the Henry constant and  $p_{O_2}$  is the partial pressure of oxygen. If we assume the validity of the ideal gas law, we can rewrite Henry's law in terms of a molar density  $c_{g,O_2} = \frac{p_{O_2}}{RT}$ . Introducing a modified Henry constant  $k_H^{cc} = \frac{k_H}{RT}$ , we get the relation  $c_{l,O_2}^* = k_H^{cc} \cdot c_{g,O_2}$  [38]. As the batch experiments have shown, the assumption of equilibrium between gas phase and liquid phase is not valid for oxygen exchange during rapid growth phases. Thus we introduce a kinetic mass transfer model depending on the difference of the actual and equilibrium concentration of oxygen in the liquid phase, a gas-liquid mass transfer capacity coefficient  $k_L \alpha$  depending on gas/liquid interfacial area (which was constant for the batch experiments) and the ratio of the phase volumes. The mass balance equations for oxygen in the liquid and gas phase are then given by

$$\frac{dc_{l,O_2}}{dt} = - \left( \frac{\mu_a}{Y_{O_2}} + m_o c_{l,O_2} \right) c_{l,O_2} + k_L \alpha \left( c_{l,O_2}^* - c_{l,O_2} \right) \quad (8c)$$

$$\frac{dc_{g,O_2}}{dt} = -k_L \alpha \left( c_{l,O_2}^* - c_{l,O_2} \right) \frac{V_l}{V_g}, \quad (8d)$$

where  $Y_{O_2}$  is the yield coefficient for oxygen and  $m_o$  is the oxygen consumption factor for maintenance.

This system of ordinary differential equations (8), together with appropriate initial conditions, specifies a modified growth rate model for *E. coli* including simultaneous aerobic and anaerobic growth, cell decay and a kinetic description for oxygen transfer. It can be customised with different models of the relative specific growth rate.

## 4. Parameter estimation

The growth model (8) developed contains a number of different parameters like maximal growth rates, half saturation constants, yield coefficients, maintenance and mass transfer coefficient etc, which need to be determined using the data obtained from the batch experiments.

Many different ways to determine the model's kinetic parameters have been developed. However, some of them are predisposed to inaccuracy and can be applied only under limited conditions. A linearisation with a Lineweaver-Burk plot was used to determine kinetic parameters, e.g. in [37, 39, 16], but this method is rather unreliable as it can greatly increase small errors in the measurements. In the last two decades, software based on non-linear regression is used to determine growth parameters, e.g. in [40, 41, 42]. In this approach a separate set of parameters is obtained for every single experiment or even for different stages of an experiment. Usually the parameters are averaged later.

In this work, we want to use a parameter estimation approach to obtain model parameters, which describe the measured quantities (like optical densities, biomass densities, DOC concentrations and oxygen concentrations in air and in water) for all experiments simultaneously. It uses an inverse model together with the initial value approach [43], [44], for details see A. The Levenberg-Marquardt-Algorithm was used to solve the optimisation problem with sensitivities derived by numerical differentiation. The forward model solves the system of equations (8) using a Runge-Kutta-Fehlberg method for systems of ordinary differential equations. The initial conditions are derived from the batch experiments.

### 4.1. Parameter estimation for the batch experiments

To combine the deviations between measured and simulated data for different measured quantities into a single objective function (15), a suitable weighting factor  $w_{ij}$  has to be chosen. In theory this should be the inverse of the measurement error. We assume that the error for each measurement is 10% of the maximal value of the measured quantity in the specific experiment.

To assess the predictive power of the growth model with the different models of the relative specific growth rate (Monod, Moser, Tessier and Contois model, (1)-(4)) a separate set of parameters was estimated each of the combinations and the residua are compared.

#### 4.1.1. Anaerobic growth

In the absence of oxygen the growth of *E. coli* is purely anaerobic ( $\mu = \mu_{an}$ ). This reduces the unknowns to the

maximum growth rate  $\mu_{max,an}$ , the anaerobic substrate yield factor  $Y_{S,an}$  and the decay rate  $r_d$ , which both are the same for all four models of the specific growth rate (1)-(4), and parameters for the growth kinetics like half saturation constant or Contois saturation constant.

The decay rate was determined from four long-run anaerobic batch experiments (6 days), each using a different dilution of the LB medium. The remaining growth parameters were estimated from 8 experiments using 4 different dilutions of the LB medium (i.e. two repetitions for each dilution) at an incubation temperature of  $21 \pm 1^\circ\text{C}$  (with a total of 125 single measurements).

#### 4.1.2. Aerobic growth

The two types of aerobic experiments emphasise different aspects. In the open system experiments the concentration of oxygen in air was kept constant with a fast air circulation (see section 2.5) and thus the mass balance equation for oxygen in the gas phase (8d) can be omitted, while the closed system experiments allow a quantification of the oxygen consumption.

A total of 334 individual measurements from 35 aerobic experiments were used to estimate the remaining 7 or 8 parameters (depending on the model used for the relative growth rate) which are only relevant in the presence of oxygen.

### 4.2. Results and Discussion

#### 4.2.1. Performance of the different growth kinetics

The residua obtained with the different models of the relative specific growth rate are given in Table 1. There was a generally good agreement between measured and simulated cell biomasses  $R_X$  and the final substrate concentrations  $R_S$  as dry biomass and substrate concentration were measured at the start of batch experiment and after the log-phase only.

The best overall agreement between simulated and measured values was obtained with the Contois model of relative specific growth. This is mostly due to a much better reproduction of the measurements of optical density and oxygen concentration in the liquid phase. The models based on a Monod, Moser or Tessier kinetic perform significantly worse. The obtained growth curves show a sharp switch between log-phase and stationary/death phase, which was not observed in the batch experiments and does not occur with the Contois kinetics. The difference is even more striking, as the Contois based model has the same amount of parameters as the models using the Monod and Tessier kinetic and one parameter less than the model with the Moser kinetic. Thus only the model with the Contois kinetic (4) is used in the rest of the paper.

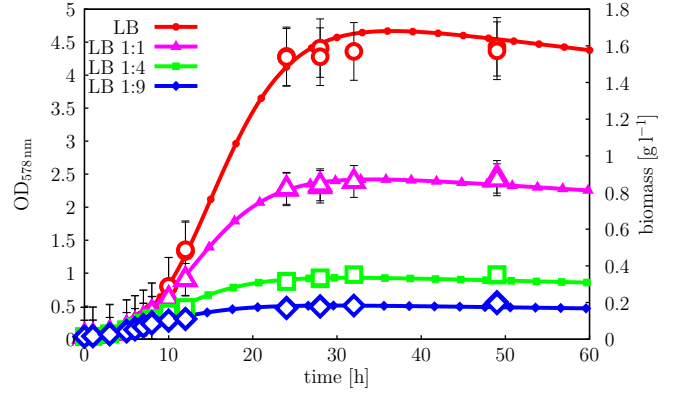


Figure 1: Comparison of OD for aerobic growth and growth curves as a solution of model (8) with estimated parameters.

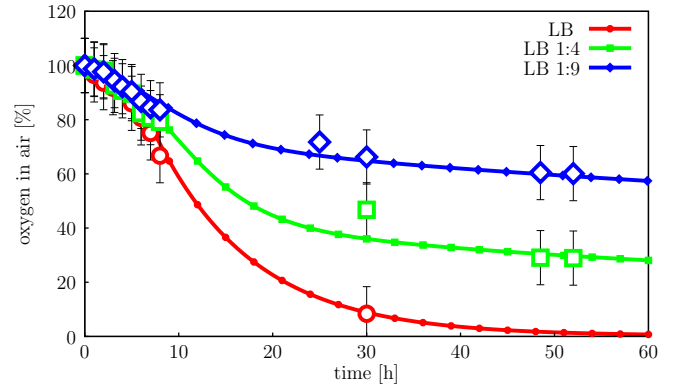


Figure 2: Comparison of measured data and oxygen concentrations in gas as a solution of model (8) with estimated parameters.

#### 4.2.2. Estimated parameters

The estimated growth parameters for the model with the Contois kinetic are given in Table 2. For all parameters the standard deviations are relatively small indicating that the model is both appropriate and not over-parametrised. Higher standard deviations for the Contois saturation constants confirm the difficulty described already in [42], where the authors mentioned that the saturation constant could vary even during a single growth cycle.

However, the agreement between simulations and experiment was very good for all types of measurements in all set-ups. As a typical example the simulated and measured biomass concentration for aerobic growth in closed serum bottles is shown in Fig. 1 for different substrate dilutions. Fig. 2 show the corresponding decrease of the oxygen concentration in the gas phase.

The estimated maximal growth rates was  $0.324 \text{ h}^{-1}$  for aerobic growth and  $0.255 \text{ h}^{-1}$  for anaerobic growth, respectively. In [42] values for  $\mu_{max,an}$  between 0.19

Table 1: Residua gained by an inverse modelling for different kinetic models

	anaerobic growth				aerobic growth					
	$R_S$	$R_{OD}$	$R_X$	$R$	$R_S$	$R_{OD}$	$R_{g,O_2}$	$R_{l,O_2}$	$R_X$	$R$
Contois	1.8	5.2	6.7	13.8	8.6	14.1	8.6	9.2	15.6	56.2
Monod	1.2	12.3	7.2	20.8	7.8	39.4	13.8	25.1	15.8	101.9
Moser	1.8	9.0	6.9	17.7	8.4	34.3	11.8	43.5	18.0	116.1
Tessier	1.4	12.9	7.2	21.5	8.4	47.4	14.9	28.0	15.2	113.8

and 0.65 in Chemostat and batch cultures at 17–20 °C were listed. [27] and [28] reported growth rates of 0.70 and 0.87 h<sup>-1</sup>, respectively for *E. coli* under optimal growth conditions in a Chemostat culture.

Comparing these values with the results of our batch experiments for aerobic growth of *E. coli*, it is obvious that the chosen growth conditions (21 ± 1 °C) and LB medium were not optimal. Under natural conditions the soil flora has to grow with a mixture of carbon sources, mostly digestion products or amino acids draining from the surface layer. The LB medium reflects naturally available carbon sources relatively well. While the DOC concentration in the LB medium is very high compared to naturally oligotrophic conditions in groundwater, an optimal nutrient supply was necessary in this study to produce measurable quantities of biomass.

The yield coefficients of 0.95 g dw per g consumable DOC and 0.49 g dw per g O<sub>2</sub> estimated for the *E. coli* cells in LB medium are also in accordance with the yield coefficients reported by [27]. Under anaerobic conditions bacteria use a mixed acid fermentation (instead of respiration) to gain energy for growth [45, 46], thus the growth is slower and the yield coefficient decreases. According to our results, a yield of 0.163 g dw per g consumable DOC was determined, which is close to the anaerobic yield coefficient of 0.18 g dw per g glucose which [39] found for some other strains of *E. coli*.

These results clearly show that it is possible to describe the growth of *E. coli* under a wide range of substrate and oxygen concentrations including both aerobic and anaerobic growth with a single set of realistic parameters.

## 5. Growth of *E. coli* in the capillary fringe

As this study is mainly targeted at the study of the growth of *E. coli* in the capillary fringe, additional experiments with Hele-Shaw cells were conducted to explore the microbial growth in a porous medium. The results of these experiments were then used to test

the transferability of the results from the batch experiments (where the micro-organisms were suspended in a liquid phase only) to a porous medium without groundwater flow.

### 5.1. Observation of bacterial growth in the capillary fringe

For the Hele-Shaw cells two 200 × 200 × 3 mm glass plates were fitted in silicone-greased spacers of 2 mm thickness on each side and filled with quartz sand (diameter: 0.35 – 0.71 mm). At the bottom of the glass cell, a stainless steel reticule (25 mm mesh size) was inserted as a carrier layer for the sterile quartz sand.

At the beginning of the experiment the initially dry quartz sand in the Hele-Shaw cells was vertically dipped 1 cm into a bacteria suspension (approx 2.4 · 10<sup>7</sup> cells ml<sup>-1</sup>) with undiluted LB medium. The chamber was kept fixed in this position for the next 3 days. A rapid rise of the water by capillary suction was observed already in the first minutes. A (hydraulic) steady state was reached after 6 hours [21]. The top of the Hele-Shaw cell was open to enable air circulation and continuous oxygen supply.

### 5.2. Cell quantification in the CF sand volume

As the suspended *E. coli* cells entered the porous medium with the rising LB medium, the concentration was assumed to be homogeneous initially and thus the cell density per volume soil resembles the profile of volumetric water content.

Based on the results of the batch experiments all consumable DOC should be depleted after 3 days either by anaerobic fermentation or by aerobic respiration. Thus after this time span the Hele-Shaw cell was lifted up from the suspension, disassembled and 1 × 1 × 0.2 cm<sup>3</sup> samples ( $n = 2$ ) of sand were taken at positions with a vertical spacing of 1 cm to count the attached and suspended *E. coli* cells.

Each air dried 0.2 cm<sup>3</sup> sand volume was transferred into 0.9 % NaCl solution and was shaken manually for several seconds [47]. Then the suspended cells were

Table 2: Growth parameters derived by inverse modelling

Parameter	Aerobic	Anaerobic
Maximum growth rate $\mu_{max}$ , [h <sup>-1</sup> ]	0.324 ± 3.7%	0.255 ± 6.9%
Decay rate $r_d$ [h <sup>-1</sup> ]	3.54 · 10 <sup>-3</sup> ± 4.2%	
Contois saturation c. $B_{S_c}$ [-]	1.81 ± 15.3%	3.07 ± 26.3%
Yield for substrate $Y_{S_c}$ [g dw g <sup>-1</sup> consumable DOC]	0.95 ± 4.3%	0.163 ± 2.1%
Contois saturation c. $B_{O_2}$ [-]	0.019 ± 27.6%	-
Yield for oxygen $Y_{O_2}$ [g dw g <sup>-1</sup> O <sub>2</sub> ]	0.49 ± 8.2%	-
Maintenance for oxygen $m_o$ [h <sup>-1</sup> g <sup>-1</sup> dw]	0.003 ± 19.9%	-
Oxygen mass transfer c. $k_L \alpha$ [h <sup>-1</sup> ]	33.2 ± 9.3%	

counted under the microscope according to [48] and the cell density was converted into cells per ml sample volume. The sample CF volume includes both the volume of the matrix and of the pore space.

The rest of the porous medium was divided into 1 cm high samples to the gravimetric water content at different heights. Using a porosity of 0.38 obtained from the dried samples, the gravimetric water content was converted into volumetric water content. A van Genuchten/Mualem model [49] with  $\alpha$  and  $n$  as free parameters and  $m = 1 - \frac{1}{n}$  was fitted to the profile to determine soil hydraulic properties.

### 5.3. Cell densities in the CF

The profile of water saturation in the Hele-Shaw cell calculated with the fitted van Genuchten model, and the vertical distribution of the cell density of *E. coli* are shown in Fig. 3. The lower part of the domain up to 2 cm is fully water saturated and the *E. coli* cells were growing anaerobically. The cell concentration in this region was  $2.2 \cdot 10^8$  cells ml<sup>-1</sup> CF volume. From the amount of bioconvertible DOC, the yield parameter  $Y_{S,an}$  estimated from the batch experiments and the cell densities, the average dry weight of one *E. coli* cell was approx.  $5.0 \cdot 10^{-13}$  g, which is in agreement with values found in the literature.

Above the water table the water content decreases with increasing height and the gas phase becomes continuous allowing for a much more efficient oxygen transport. This allows aerobic growth and thus a better substrate utilisation. The highest cell densities (up to  $6.5 \cdot 10^8$  cells ml<sup>-1</sup> CF volume) were observed in a region with a water content between 0.5 and 0.8, as here a optimal balance between the availability of substrate and oxygen was obtained for the *E. coli* cells. Above this zone the cell density decreases proportional to the water content.

### 5.4. Reactive transport model

Microbial growth in an unsaturated porous medium can be simulated as a special kind of reactive multiphase flow. For each component  $\kappa$  a mass balance equation is given by

$$\frac{\partial(\theta_\alpha c_{\alpha,\kappa})}{\partial t} + \nabla \cdot \{j_{\alpha,\kappa}\} = r_{\alpha,\kappa} + e_{\alpha,\kappa}, \quad (9)$$

where  $\theta_\alpha = s_\alpha \phi$  is the volumetric water or gas content depending on the phase saturation  $s_\alpha$  and the porosity  $\phi$ ,  $c_{\alpha,\kappa}$  is the concentration of component  $\kappa$  in phase  $\alpha$ ,  $j_{\alpha,\kappa}$  is the flux of component  $\kappa$  in phase  $\alpha$ ,  $r_{\alpha,\kappa}$  is the net change by reactions and  $e_{\alpha,\kappa}$  is the phase exchange. The main components of the system are oxygen, consumable DOC as a dissolved substrate and the microbial cell density (the two latter only occur in the liquid phase).

Due to the high diffusion coefficient for oxygen in the gas phase and the small solubility, we assume that pressure changes due to the reactions are negligible and gas transport is purely diffusive. In the absence of groundwater flow the solute is also transported by diffusion only. We assume that *E. coli* cells are immotile and thus do not move without water flow, therefore  $j_{l,x}$  can be neglected.

Ficks' law is used together with the second model of Millington and Quirk for the dependence of the effective diffusion coefficient on phase saturation [50] and one obtains

$$j_{\alpha,\kappa} = -s_\alpha^2 \phi^{\frac{4}{3}} D_{\alpha,\kappa} \nabla c_{\alpha,\kappa},$$

where  $D_{\alpha,\kappa}$  is the molecular diffusion coefficient of component  $\kappa$  in phase  $\alpha$ .

With the growth model (8) derived from the batch experiments we obtain the following reaction terms for cell density  $c_{l,x}$  and substrate and oxygen concentra-



tion  $c_{l,S}, c_{l,O_2}$ :

$$\begin{aligned} r_{l,X} &= \theta_l (\mu_a + \mu_{an} - r_d) c_{l,X}, \\ r_{l,S} &= -\theta_l \left( \frac{\mu_a}{Y_{S,a}} + \frac{\mu_{an}}{Y_{S,an}} \right) c_{l,X}, \\ r_{l,O_2} &= -\theta_l \left( \frac{\mu_a}{Y_{O_2}} + m_o c_{l,O_2} \right) c_{l,X}. \end{aligned}$$

### 5.5. Oxygen phase exchange in porous media

To describe the non-equilibrium mass transfer of oxygen between gas and liquid phase, we follow a model discussed in [51] and [52] based on a stagnant film model originally developed for spherical gas bubbles. A similar approach was also used for the dissolution of a nonaqueous phase liquid by [53].

In this model it is assumed that the mass transfer rate  $e_{g,O_2}/e_{l,O_2}$  between both phases is proportional to the difference between the concentration of oxygen in the liquid phase  $c_{l,O_2}$  and its equilibrium value  $c_{l,O_2}^*$ , and the specific area of the water-air interface  $a_{gw}$  and thus is given by

$$-e_{g,O_2} = e_{l,O_2} = \beta a_{gw} (c_{l,O_2}^* - c_{l,O_2}), \quad (10)$$

where  $\beta$  is a proportionality constant called mass transfer coefficient.

In case of no flow, the mass transfer coefficient  $\beta$  for a spherical structure with a mean particle diameter  $p_d$  is given by [54]

$$\beta = \frac{1}{\delta_{\text{eff}}} D_{l,O_2} = \left( \frac{2}{p_d} + \frac{1}{\delta} \right) D_{l,O_2}, \quad (11)$$

where  $D_{l,O_2}$  is the oxygen diffusion coefficient in water and  $\delta$  is the thickness of the stagnant film layer. In no-flow conditions, the term  $2p_d^{-1}$  dominates and the effective boundary layer thickness  $\delta_{\text{eff}}$  is therefore proportional to  $p_d$  [52].

For this approach the determination of the gas-liquid interfacial area is a crucial parameter. Many (empirical) relationships are proposed in literature, for an overview see [55].

A rather simple model - based on geometrical considerations- to estimate the total surface area for any packing of spheres was presented by [56]. They claim that the effective interfacial area is proportional to the gas saturation and is given by

$$a_{gw} = \kappa s_g \frac{6\phi}{p_d}, \quad (12)$$

where  $\kappa$  should describe the fraction of the liquid-gas surface area exposed to mobile water. It is often assumed to be equal to the porosity [51].

A more complex approach to determine the gas-liquid interfacial area using an equivalent pore size distribution derived from the water retention function was proposed by [57] and [58]. The effective air-water interfacial area is the given by

$$a_{gw} = \frac{3\phi}{2\sigma} \int_0^{s_l} p_c(S) dS, \quad (13)$$

where  $\sigma$  is the surface tension of the water. The integral in (13) can be calculated analytically for a van Genuchten parametrisation [49] with  $m = 1 - \frac{1}{n}$  using the substitution  $z = \frac{n+1}{n}$ ,  $w = \frac{n-2}{n}$  (see [58], eq. (15)) and (13) can be expressed as

$$a_{gw} = \frac{3\phi}{2\sigma} \frac{n-1}{\alpha n} B(w, z) (1 - I_u(w, z)), \quad (14)$$

where  $B(w, z)$  is the beta function and  $I_u(w, z)$  represents the incomplete beta function.

#### 5.5.1. Numerical discretisation

The system of reaction-diffusion equations (9) was discretised using a cell-centered finite-volume scheme in space and an implicit Euler scheme in time. The arising non-linear equations are solved with Newton-Method. The DUNE/PDELab software framework [59, 60] was used to facilitate the implementation.

As the flow process in the Hele-Shaw cell was essentially vertical, a one-dimensional grid with a 1024 cells was used, which produced a grid convergent solution.

### 5.6. Numerical simulation of growth in porous media

As the initial infiltration and the establishment of a stationary CF was fast (compared to the duration of the experiment) and no changes in water saturation were observed afterwards, we can assume that the consumable DOC and *E. coli* concentrations at the beginning of the experiment are uniform. The initial concentrations of all components are given in Table 3.

All domain boundaries were assumed to be impermeable for components in the liquid phase (zero-flux Neumann boundary condition). As the Hele-Shaw cell was open at the top, a Dirichlet boundary condition was used for oxygen in the gas phase with a mass fraction of 20.95% and standard pressure and temperature.

For the growth model the parameters determined in the batch experiments were used (Table 2). As described above the hydraulic parameters were obtained by independent measurements (Section 5.3) and the diffusion coefficients were taken from literature (Table 4). No additional calibration was performed.

A comparison of profiles of simulated and measured cell densities is shown in Fig. 3. The simulated cell

Table 3: Initial concentrations of liquid and gas component

Component	Initial concentration
biomass $c_{l,X}$	$12 \text{ mg l}^{-1}$
consumable substrate $c_{l,S}$	$2.0 \text{ g l}^{-1}$
dissolved oxygen in water $c_{l,O_2}$	$3.0 \text{ mg l}^{-1}$
oxygen in air $c_{g,O_2}$	$8.7 \text{ mmol l}^{-1}$

Table 4: Hydraulic parameters and diffusion coefficients for the sample calculations

van Genuchten model	
$n$	4.9
$\alpha$	$1.7 \cdot 10^{-3} \text{ Pa}^{-1}$
porosity $\phi$	
	0.38
Diffusion coefficients	
$\dagger D_{l,S}$	$1.9 \cdot 10^{-10} \text{ m}^2 \text{ s}^{-1}$
$\ddagger D_{l,O_2}$	$2.2 \cdot 10^{-9} \text{ m}^2 \text{ s}^{-1}$
$\ddagger D_{g,O_2}$	$1.8 \cdot 10^{-5} \text{ m}^2 \text{ s}^{-1}$
$\dagger$ [61], $\ddagger$ [62]	

density is very sensitive to the model used to represent the phase exchange of oxygen for water saturations between 0.5 and 0.95, whereas in the completely water saturated part of the Hele-Shaw cell growth is always anaerobic and at a water saturation below 0.5 oxygen diffusion in the continuous gas phase and phase exchange are always fast enough and thus growth is purely aerobic.

For both models of oxygen transfer, the efficiency of the phase exchange decreases with increasing mean particle diameter  $p_d$ . Thus for smaller values of  $p_d$  the position of the peak of the cell density is shifted to lower water saturations (higher positions) and is at the same time decreasing in height due to the reduced amount of substrate available at lower water saturations. While for the Niemet model (14) a good agreement between measured and simulated values is obtained with  $r_d = 0.35 \text{ mm}$  (which is the size of the smaller grains in the sand used), a sufficient match for the simpler model Gvirtzman and Roberts (12) requires an unrealistically large value of  $r_d = 1.2 \text{ mm}$ .

In both models (12) and (14) the gas-liquid interfacial area is roughly proportional to the air content. However, the network models [63, 64, 65] and experiments with glass beads [66, 55] found this relationship to hold only for  $s_l > 0.3$ . The air-water interfacial area can decrease again for lower water saturations, which would result in an overestimated phase exchange (and aerobic growth). This could explain the slightly to high biomass in the region with low water saturations. However, as oxygen is not the limiting factor under these

conditions this is rather unlikely.

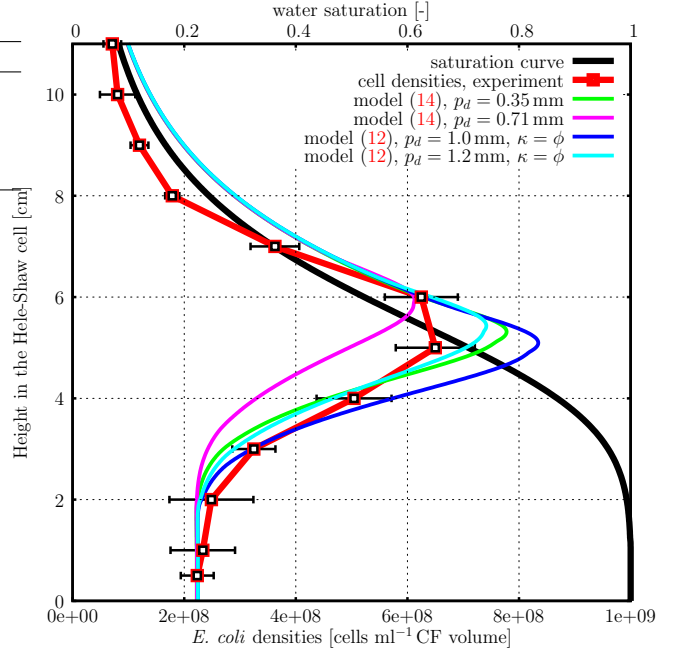


Figure 3: Comparison of cell density concentration computed by a numerical simulation for different oxygen exchange models with the experimental data after 3 days of growth in LB medium.

## 6. Conclusions

*E. coli* in faeces naturally grows under anaerobic conditions by mixed acid fermentation [26], but it can also grow by respiration e.g. in Chemostat cultures under aeration. Based on experiments in batch culture, we developed a mathematical model, which is able to consider both, the aerobic and the anaerobic growth of *E. coli*.

A suitable growth model for *E. coli* (HB101 K12 pGLO) based on laboratory experiments in batch culture was developed. The model is able to consider both, aerobic and anaerobic growth simultaneously. Using different types of data from many batch experiments, a unique set of growth parameters describing all batch experiments was determined using inverse modelling.

From a series of alternative growth rate models, the modified growth rate model proposed by [33] resulted in the best agreement between measured and simulated data.

The proposed model for microbiological growth of *E. coli* in batch cultures was extended with models for the oxygen phase exchange and transport of substrate and oxygen to be able to describe growth in porous media.

Results of the laboratory experiment in a Hele-Shaw cell filled with quartz sand and of modelling of cell distribution showed a very good prediction of the cell density profile of *E. coli* cells within the CF. The numerical simulation was performed without any additional calibration of the parameters estimated from the batch experiments. While the numerical simulation showed a strong dependency on the model used to calculate air-water interfacial area, the model of Niemet produced a very good agreement with the counted cell densities using the particle diameter of the smaller grains in the sand used in the experiment.

The very good predictive quality of the growth model developed from batch experiments for the quite different conditions in a porous medium makes it a promising basis for further experiments. While the model was applied in this work only to bacterial growth under static conditions, it will be applied to situations with groundwater flow and continuous nutrient supply in the future.

### A. Parameter Estimation

The temporal development of a dynamic system with the components  $x_1, \dots, x_n$  is given by a system of ordinary differential equations (in vector notation)

$$\frac{d\mathbf{x}}{dt} = \mathbf{f}(\mathbf{x}; \boldsymbol{\theta}; t) \quad \mathbf{x}(0) = \mathbf{x}_0$$

with  $\mathbf{x} = (x_1, \dots, x_n)^T$  and parameters  $\boldsymbol{\theta} = (\theta_1, \dots, \theta_p)^T$ . Let  $y_{i,j}$  denote measurements (or functions of the measurements) taken at time points  $t_j, j = 1, \dots, m$ .

The problem to be solved is the minimization of the objective function (residuum)

$$R(\boldsymbol{\theta}) = \sum_{i=1}^n R_i(\boldsymbol{\theta}) = \sum_{i=1}^n \sum_{j=1}^m \left( \frac{x_{ij}(\boldsymbol{\theta}, t) - y_{ij}}{w_{ij}} \right)^2 \quad (15)$$

over the set of admissible parameter values with appropriate weighting factors  $w_{ij}$ .

### Acknowledgements

This study was funded by DFG (German Research Foundation) through the Research Group FOR 831 "Dynamic Capillary Fringes: A Multidisciplinary Approach" (Project Ga 546/5-2 and Ba 1498/7-2). Furthermore, we thank D. Bonafas for his excellent laboratory assistance.

### References

- [1] Cannavo, P., Richaume, a., Lafolie, F.: Fate of nitrogen and carbon in the vadose zone: in situ and laboratory measurements of seasonal variations in aerobic respiratory and denitrifying activities. *Soil Biology and Biochemistry* **36**(3), 463–478 (2004). DOI 10.1016/j.soilbio.2003.10.023. URL <http://linkinghub.elsevier.com/retrieve/pii/S0038071703003511>
- [2] Holden, P., Fierer, N.: Microbial processes in the vadose zone. *Vadose Zone Journal* **4**(1), 1–21 (2005). DOI 10.2136/vzj2005.0001. URL <http://vzj.geoscienceworld.org/content/4/1/1.short>
- [3] Or, D., Smets, B., Wraith, J., Dechesne, A., Friedman, S.: Physical constraints affecting bacterial habitats and activity in unsaturated porous media - a review. *Advances in Water Resources* **30**(6-7), 1505–1527 (2007). DOI 10.1016/j.advwatres.2006.05.025. URL <http://linkinghub.elsevier.com/retrieve/pii/S030917080600131X>
- [4] Dechesne, A., Or, D., Gülez, G., Smets, B.F.: The porous surface model, a novel experimental system for online quantitative observation of microbial processes under unsaturated conditions. *Applied and Environmental Microbiology* **74**(16), 5195–200 (2008). DOI 10.1128/AEM.00313-08. URL <http://www.pubmedcentral.nih.gov/articlerender.fcgi?artid=2519293&tool=pmcentrez&rendertype=abstract>
- [5] Tindall, J., Weeks, E., Friedel, M.: Part 2: A field study of enhanced remediation of toluene in the vadose zone using a nutrient solution. *Water, Air, and Soil Pollution* **168**(1-4), 359–389 (2005). DOI doi:10.1007/s11270-005-3584-4. URL <http://www.ingentaconnect.com/content/klu/wate/2005/00000168/F0040001/00003584>
- [6] Lee, E.J., Kim, M., Kim, Y., Lee, K.K.: Numerical and field investigation of enhanced in situ denitrification in a shallow-zone well-to-well recirculation system. *Ecological Modelling* **220**(19), 2441–2449 (2009). DOI 10.1016/j.ecolmodel.2009.06.014. URL <http://linkinghub.elsevier.com/retrieve/pii/S0304380009003913>
- [7] Bester, K., Banzhaf, S., Burkhardt, M., Janzen, N., Niederstrasser, B., Scheytt, T.: Activated soil filters for removal of biocides from contaminated runoff and waste-waters. *Chemosphere* **85**(8), 1233–40 (2011). DOI 10.1016/j.chemosphere.2011.07.017. URL <http://www.ncbi.nlm.nih.gov/pubmed/21855108>
- [8] Ronen, D., Scher, H., Blunt, M.: On the structure and flow processes in the capillary fringe of phreatic aquifers. *Transport in Porous Media* **28**(2), 159–180 (1997). DOI 10.1023/A:1006583410617. URL <http://dx.doi.org/10.1023/A%3A1006583410617>
- [9] Skopp, J., Jawson, M., Doran, J.: Steady-state aerobic microbial activity as a function of soil water content. *Soil Science Society of America Journal* **54**(6), 1619–25 (1990). DOI 10.2136/sssaj1990.03615995005400060018x. URL <https://www.crops.org/publications/sssaj/abstracts/54/6/SS0540061619>
- [10] Chang, W., Halverson, L.: Reduced water availability influences the dynamics, development, and ultrastructural properties of *Pseudomonas putida* biofilms.

- Journal of Bacteriology **185**(20), 6199–6204 (2003). DOI 10.1128/JB.185.20.6199-6204.2003. URL <http://j.b.asm.org/content/185/20/6199.short>
- [11] Trevors, J.: Respiratory activity of a genetically engineered *Pseudomonas fluorescens* strain in soil measured using gas chromatography. Journal of Microbiological Methods **14**(1), 11–20 (1991). URL <http://www.sciencedirect.com/science/article/pii/0167701291900039>
- [12] Bell, C., McIntyre, N., Cox, S., Tissue, D., Zak, J.: Soil microbial responses to temporal variations of moisture and temperature in a chihuahuan desert grassland. Microbial Ecology **56**(1), 153–67 (2008). DOI 10.1007/s00248-007-9333-z. URL <http://www.ncbi.nlm.nih.gov/pubmed/18246293>
- [13] Fernández-Calviño, D., Rousk, J., Brookes, P.C., Bååth, E.: Bacterial pH-optima for growth track soil pH, but are higher than expected at low pH. Soil Biology and Biochemistry **43**(7), 1569–1575 (2011). DOI 10.1016/j.soilbio.2011.04.007. URL <http://linkinghub.elsevier.com/retrieve/pii/S0038071711001659>
- [14] Borch, T., Kretzschmar, R., Kappler, A., Cappellen, P.V., Ginder-Vogel, M., Voegelin, A., Campbell, K.: Biogeochemical redox processes and their impact on contaminant dynamics. Environmental Science & Technology **44**(1), 15–23 (2010). DOI 10.1021/es9026248. URL <http://www.ncbi.nlm.nih.gov/pubmed/20000681>
- [15] Reischke, S., Rousk, J., Bååth, E.: The effects of glucose loading rates on bacterial and fungal growth in soil. Soil Biology and Biochemistry **70**, 88–95 (2013). DOI 10.1016/j.soilbio.2013.12.011. URL <http://linkinghub.elsevier.com/retrieve/pii/S0038071713004446>
- [16] Sierra, J., Renault, P.: Oxygen consumption by soil microorganisms as affected by oxygen and carbon dioxide levels. Applied Soil Ecology **2**(3), 175–184 (1995). DOI 10.1016/0929-1393(95)00051-L. URL <http://linkinghub.elsevier.com/retrieve/pii/092913939500051L>
- [17] Limmer, C., Drake, H.: Effects of carbon, nitrogen, and electron acceptor availability on anaerobic N<sub>2</sub>-fixation in a beech forest soil. Soil Biology and Biochemistry **30**(2), 153–158 (1998). DOI 10.1016/S0038-0717(97)00099-0. URL <http://www.sciencedirect.com/science/article/pii/S0038071797000990>
- [18] Bundt, M., Widmer, F., Pesaro, M.: Preferential flow paths: biological 'hot spots' in soils. Soil Biology and Biochemistry **33**(1), 729–38 (2001). URL <http://www.sciencedirect.com/science/article/pii/S0038071700002182>
- [19] Affek, H.P., Ronen, D., Yakir, D.: Production of CO<sub>2</sub> in the capillary fringe of a deep phreatic aquifer. Water Resources Research **34**(5), 989–996 (1998). DOI 10.1029/98WR00095. URL <http://dx.doi.org/10.1029/98WR00095>
- [20] Jost, D., Winter, J., Gallert, C.: Distribution of aerobic motile and non-motile bacteria within the capillary fringe of silica sand. Water Research **44**(4), 1279–87 (2010). DOI 10.1016/j.watres.2010.01.001. URL <http://www.ncbi.nlm.nih.gov/pubmed/20116084>
- [21] Jost, D., Winter, J., Gallert, C.: Water and Oxygen Dependence of *Pseudomonas putida* Growing in Silica Sand Capillary Fringes. Vadose Zone Journal **10**(2), 532 (2011). DOI 10.2136/vzj2010.0092. URL <http://vzj.geoscienceworld.org/cgi/content/abstract/10/2/532>
- [22] Bauer, R.D., Maloszewski, P., Zhang, Y., Meckenstock, R.U., Griebler, C.: Mixing-controlled biodegradation in a toluene plume—results from two-dimensional laboratory experiments. Journal of Contaminant Hydrology **96**(1-4), 150–68 (2008). DOI 10.1016/j.jconhyd.2007.10.008. URL <http://www.ncbi.nlm.nih.gov/pubmed/18083271>
- [23] Bauer, R.D., Rolle, M., Kürzinger, P., Grathwohl, P., Meckenstock, R.U., Griebler, C.: Two-dimensional flow-through microcosms - Versatile test systems to study biodegradation processes in porous aquifers. Journal of Hydrology **369**(3-4), 284–295 (2009). DOI 10.1016/j.jhydrol.2009.02.037. URL <http://linkinghub.elsevier.com/retrieve/pii/S0022169409001164>
- [24] Chen, G., Walker, S.L.: Fecal indicator bacteria transport and deposition in saturated and unsaturated porous media. Environmental Science & Technology **46**(16), 8782–90 (2012). DOI 10.1021/es301378q. URL <http://www.ncbi.nlm.nih.gov/pubmed/22809290>
- [25] Clark, D.: The fermentation pathways of *Escherichia coli*. FEMS Microbiology Letters **63**(3), 223–234 (1989). DOI 10.1111/j.1574-6968.1989.tb03398.x. URL <http://www.sciencedirect.com/science/article/pii/0378109789901328>
- [26] Madigan, M.T., Martinko, J.M., Stahl, D., Clark, D.P.: Brock Biology of Microorganisms, 13 edn. Benjamin Cummings (2010)
- [27] Reiling, H., Laurila, H., Fiechter, a.: Mass culture of *Escherichia coli*: Medium development for low and high density cultivation of *Escherichia coli* B/r in minimal and complex media. Journal of Biotechnology **2**(3-4), 191–206 (1985). DOI 10.1016/0168-1656(85)90038-0. URL <http://linkinghub.elsevier.com/retrieve/pii/0168165685900380>
- [28] Lendenmann, U., Egli, T.: Is *Escherichia coli* growing in glucose-limited chemostat culture able to utilize other sugars without lag? Microbiology (Reading, England) **141** ( Pt 1)(1 995), 71–8 (1995). URL <http://www.ncbi.nlm.nih.gov/pubmed/7894722>
- [29] Larsson, G., Enfors, S.: Kinetics of *Escherichia coli* hydrogen production during short term repeated aerobic-anaerobic fluctuations. Bioprocess Engineering **9**(4), 167–172 (1993). URL <http://link.springer.com/article/10.1007/BF00389925>

- [30] Haberer, C.: Oxygen transfer in a fluctuating capillary fringe. *Journal of Contaminant Hydrology* **122**(1-4), 26–39 (2011). DOI 10.1016/j.jconhyd.2010.10.006. URL <http://www.ncbi.nlm.nih.gov/pubmed/21131093>
- [31] Monod, J.: The growth of bacterial cultures. *Annual Reviews in Microbiology* **3** (1949). URL <http://www.annualreviews.org/doi/abs/10.1146/annurev.mi.03.100149.002103>
- [32] Moser, H.: The dynamics of bacterial populations maintained in the chemostat. Carnegie Institution of Washington Washington (1958)
- [33] Contois, D.E.: Kinetics of bacterial growth: relationship between population density and specific growth rate of continuous cultures. *Journal of General Microbiology* **21**, 40–50 (1959). URL <http://www.ncbi.nlm.nih.gov/pubmed/13811643>
- [34] Powell, E., Evans, C., Strange, E., Tempest, D.: *Microbial physiology and continuous culture*. HMSO, London (1967)
- [35] Dabes, J.N., Finn, R.K., Welke, C.R.: Equations of substrate-limited growth: the case for Blackman kinetics. *Biotechnology and Bioengineering* **15**(6), 1159–77 (1973). DOI 10.1002/bit.260150613. URL <http://www.ncbi.nlm.nih.gov/pubmed/4203180>
- [36] Koch, A., Wang, C.: How close to the theoretical diffusion limit do bacterial uptake systems function? *Archives of Microbiology* **131**(1), 36–42 (1982). DOI 10.1007/BF00451496. URL <http://link.springer.com/article/10.1007/BF00451496>
- [37] Kornaros, M., Lyberatos, G.: Kinetics of aerobic growth of a denitrifying bacterium, *Pseudomonas denitrificans*, in the presence of nitrates and/or nitrites. *Water Research* **31**(3), 479 – 488 (1997). DOI 10.1016/S0043-1354(96)00288-6. URL <http://www.sciencedirect.com/science/article/pii/S0043135496002886>
- [38] Sander, R.: *Compilation of Henry’s Law Constants for Inorganic and Organic Species of Potential Importance in Environmental Chemistry (Version 3)* (1999). URL <http://www.henrys-law.org/>
- [39] Ataai, M., Shuler, M.: Simulation of the growth pattern of a single cell of *Escherichia coli* under anaerobic conditions. *Biotechnology and Bioengineering* **27**(8), 1027–1035 (1985). URL <http://onlinelibrary.wiley.com/doi/10.1002/bit.260270714/abstract>
- [40] Senn, H., Lendenmann, U., Snozzi, M.: The growth of *Escherichia coli* in glucose-limited chemostat cultures: a re-examination of the kinetics. *Biochimica et Biophysica Acta* **1201**(3), 424–436 (1994). URL <http://www.sciencedirect.com/science/article/pii/0304416594900728>
- [41] Kovárová, K., Zehnder, A.J., Egli, T.: Temperature-dependent growth kinetics of *Escherichia coli* ML 30 in glucose-limited continuous culture. *Journal of Bacteriology* **178**(15), 4530–9 (1996). URL <http://www.pubmedcentral.nih.gov/articlerender.fcgi?artid=178220&tool=pmcentrez&rendertype=abstract>
- [42] Kovárová-Kovar, K., Egli, T.: Growth kinetics of suspended microbial cells: from single-substrate-controlled growth to mixed-substrate kinetics. *Microbiology and Molecular Biology Reviews* **62**(3), 646–666 (1998). URL <http://mmb.asm.org/content/62/3/646.short>
- [43] Richter, O., Söndgerath, D.: *Parameter estimation in ecology: the link between data and models*. VCH Verlagsgesellschaft, Weinheim, Germany (1990)
- [44] Marsili-Libelli, S.: Parameter estimation of ecological models. *Ecological Modelling* **62**(4), 233–258 (1992). DOI 10.1016/0304-3800(92)90001-U. URL <http://www.sciencedirect.com/science/article/pii/030438009290001U>
- [45] Stokes, J.: Fermentation of glucose by suspensions of *Escherichia coli*. *Journal of Bacteriology* **57**(2), 147–158 (1949). URL <http://www.ncbi.nlm.nih.gov/pmc/articles/PMC385489/>
- [46] Paegle, L., Gibbs, M.: Anaerobic dissimilation of glucose-C14 by *Escherichia coli*. *Journal of Bacteriology* **81**(1), 107–110 (1961)
- [47] Jost, D., Winter, J., Gallert, C.: Non-invasive quantification of gfp-labeled *Escherichia coli* in the capillary fringe by fluorescence intensity (2014). Submitted in *Vadose Zone Journal*
- [48] Taylor, J., Wilson, B., Mills, M., Burns, R.: Comparison of microbial numbers and enzymatic activities in surface soils and subsoils using various techniques. *Soil Biology and Biochemistry* **34**(3), 387 – 401 (2002). DOI 10.1016/S0038-0717(01)00199-7
- [49] Genuchten, M.V.: A closed-form equation for predicting the hydraulic conductivity of unsaturated soils. *Soil Science Society of America Journal* **44**, 892–8 (1980). URL <https://dl.sciencesocieties.org/publications/sssaj/abstracts/44/5/SS0440050892>
- [50] Jin, Y., Jury, W.: Characterizing the dependence of gas diffusion coefficient on soil properties. *Soil Science Society of America Journal* **60**(1), 66–71 (1996). DOI 10.2136/sssaj1996.03615995006000010012x. URL <https://www.soils.org/publications/sssaj/abstracts/60/1/SS0600010066https://dl.sciencesocieties.org/publications/sssaj/abstracts/60/1/SS0600010066>
- [51] Geistlinger, H., Beckmann, A., Lazik, D.: Mass transfer between a multicomponent trapped gas phase and a mobile water phase: Experiment and theory. *Water Resources Research* **41**(11) (2005). DOI 10.1029/2004WR003885. URL <http://dx.doi.org/10.1029/2004WR003885>
- [52] Holocher, J., Peeters, F., Aeschbach-Hertig, W., Kinzelbach, W., Kipfer, R.: Kinetic Model of Gas Bubble Dissolution in Groundwater and Its Implications for the Dissolved Gas Composition. *Environmental*

- Science & Technology **37**(7), 1337–1343 (2003). DOI 10.1021/es025712z. URL <http://pubs.acs.org/doi/abs/10.1021/es025712z>
- [53] Mayer, A.S., Miller, C.T.: The influence of mass transfer characteristics and porous media heterogeneity on nonaqueous phase dissolution. *Water Resources Research* **32**(6), 1551–1567 (1996). DOI 10.1029/96WR00291. URL <http://doi.wiley.com/10.1029/96WR00291>
- [54] Clift, R., Grace, J.R., Weber, M.E.: *Bubbles, drops, and particles*. Academic Press Inc., New York (1978)
- [55] Porter, M.L., Wildenschild, D., Grant, G., Gerhard, J.I.: Measurement and prediction of the relationship between capillary pressure, saturation, and interfacial area in a napl-water-glass bead system. *Water Resources Research* **46**(8) (2010). DOI 10.1029/2009WR007786. URL <http://dx.doi.org/10.1029/2009WR007786>
- [56] Gvirtsman, H., Roberts, P.V.: Pore scale spatial analysis of two immiscible fluids in porous media. *Water Resources Research* **27**(6), 1165–1176 (1991). DOI 10.1029/91WR00303. URL <http://onlinelibrary.wiley.com/doi/10.1029/91WR00303/full>
- [57] Cary, J.: Estimating the surface area of fluid phase interfaces in porous media. *Journal of Contaminant Hydrology* **15**(4), 243–248 (1994). DOI 10.1016/0169-7722(94)90029-9. URL <http://linkinghub.elsevier.com/retrieve/pii/0169772294900299>
- [58] Niemet, M.R., Rockhold, M.L., Weisbrod, N., Selker, J.S.: Relationships between gas-liquid interfacial surface area, liquid saturation, and light transmission in variably saturated porous media. *Water Resources Research* **38**(8), 10–1–10–12 (2002). DOI 10.1029/2001WR000785. URL <http://doi.wiley.com/10.1029/2001WR000785>
- [59] Bastian, P., Blatt, M., Dedner, A., Engwer, C., Klöfkom, R., Kornhuber, R., Ohlberger, M., Sander, O.: A generic grid interface for parallel and adaptive scientific computing. Part II: implementation and tests in dune. *Computing* **82**(2-3), 121–138 (2008). DOI 10.1007/s00607-008-0004-9. URL <http://dx.doi.org/10.1007/s00607-008-0004-9>
- [60] Bastian, P., Heimann, F., Marnach, S.: Generic implementation of finite element methods in the distributed and unified numerics environment (DUNE). *Kybernetika* **46**(2), 294–315 (2010)
- [61] Hendry, M.J., Ranville, J.R., Boldt-Leppin, B.E.J., Wassenaar, L.I.: Geochemical and transport properties of dissolved organic carbon in a clay-rich aquitard. *Water Resources Research* **39**(7) (2003). DOI 10.1029/2002WR001943. URL <http://dx.doi.org/10.1029/2002WR001943>
- [62] Aachib, M., Mbonimpa, M., Aubertin, M.: Measurement and Prediction of the Oxygen Diffusion Coefficient in Unsaturated Media, with Applications to Soil Covers. *Water, Air, & Soil Pollution* **156**(1), 163–193 (2004). DOI 10.1023/B:WATE.0000036803.84061.e5. URL <http://link.springer.com/10.1023/B:WATE.0000036803.84061.e5>
- [63] Reeves, P.C., Celia, M.: A Functional Relationship Between Capillary Pressure, Saturation, and Interfacial Area as Revealed by a Pore-Scale Network Model. *Water Resources Research* **32**(8), 2345–2358 (1996). DOI 10.1029/96WR01105. URL <http://doi.wiley.com/10.1029/96WR01105>
- [64] Held, R.J., Celia, M.: Modeling support of functional relationships between capillary pressure, saturation, interfacial area and common lines. *Advances in Water Resources* **24**(3-4), 325–343 (2001). DOI 10.1016/S0309-1708(00)00060-9. URL <http://linkinghub.elsevier.com/retrieve/pii/S0309170800000609>
- [65] Joekar-Niasar, V., Hassanizadeh, S.M., Leijnse, A.: Insights into the Relationships Among Capillary Pressure, Saturation, Interfacial Area and Relative Permeability Using Pore-Network Modeling. *Transport in Porous Media* **74**(2), 201–219 (2007). DOI 10.1007/s11242-007-9191-7. URL <http://link.springer.com/10.1007/s11242-007-9191-7>
- [66] Culligan, K.A., Wildenschild, D., Christensen, B.S.B., Gray, W.G., Rivers, M.L., Tompson, A.F.B.: Interfacial area measurements for unsaturated flow through a porous medium. *Water Resources Research* **40**(12), W12,413/1–W12,413/12 (2004). DOI 10.1029/2004WR003278. URL <http://doi.wiley.com/10.1029/2004WR003278>